Evidence of optical circular dichroism in GaAs-based nanowires partially covered with gold

*Grigore Leahu, Emilija Petronijevic, Alessandro Belardini, Marco Centini, Concita Sibilia *,
Teemu Hakkarainen, Eero Koivusalo, Marcelo Rizzo Piton, Soile Suomalainen, Mircea Guina*

G. Leahu, E. Petronijevic, A. Belardini, M. Centini, C. Sibilia
Sapienza University of Rome, SBAI Department, Via Antonio Scarpa 16 Rome, 00161, Italy.
E-mail: concita.sibilia@uniroma1.it

T. Hakkarainen, E. Koivusalo, M. Rizzo Piton, S. Suomalainen, M. Guina
Optoelectronics Research Centre, Tampere University of Technology, Korkeakoulunkatu 3,
33720 Tampere, Finland.

M. Rizzo Piton,
Departamento de Física, Universidade Federal de São Carlos, CP 676, São Carlos, SP, Brazil.

Semiconductor nanostructures hybridized with metals have been known to offer new

opportunities in nonlinear optics, plasmonics, lasing, biosensors; among them GaAs-based

nanowires (NWs) hybridized with gold could offer new functionalities, as chiral sensing and

light manipulation, as well as circular polarization sources. We investigated GaAs-AlGaAs-

GaAs NWs fabricated by self-catalyzed growth on Si substrates, and partially covered with

gold, thus inducing the symmetry breaking and a potential chiral response. Three different

samples are investigated, each of them with a different morphology, as the length and the

overall diameter ranging from 4.6 to 5.19μm and from 138 up to165nm, respectively. The

samples are firstly characterized by measuring the absorption spectra by using a scattering-

free photo-acoustic (PA) technique. Then the circular dichroism (CD) is investigated by

measuring PA absorption for circularly polarized light under different incident angles at 532

nm and 980 nm. An efficient CD is found for proper configurations, and results are in good

agreement with extrinsic chiral theory predictions and numerical simulations. It is therefore proven that these samples exhibit chiral behavior, and can be further optimized. Moreover, PA technique can be used as an extremely sensitive and efficient technique to characterize their "extrinsic" chirality.

1. Introduction

Nanostructures with broken symmetry put in interaction with circularly polarized light can mimic the chiral response present in important molecules and DNA. Engineering these structures thus paves the way for the important applications spreading from negative refraction [1-3], chiral sensing [4,5] to production of optical field carrying out optical angular momentum for quantum information applications [6]. It has been shown that plasmonic nanostructures forming 1D [7] elements, 2D metasurfaces [8-10], and 3D metamaterials [11] can exhibit linear chiral response due to their own, intrinsic chirality. Also semiconductor nanostructures can exhibit chiral features [12-16]. From the optical point of view, chiral structures possess the ability to rotate the plane of polarization of electromagnetic waves (optical activity), and give rise to circular dichroism - the property of absorbing by different amounts the right and left-handed circular polarization.

Apart from 3D chiral objects, the possibility to obtain optical chirality, i.e. optical activity, with non-chiral elements was studied in the past [17], but only recently reconsidered [18,19]. This phenomenon is obtained when the experimental configuration composed by both the non-chiral object and the optical incident field is non-superimposable on its mirror image [20]. This is called "extrinsic" chirality; in our previous works we have investigated this type of chirality in tilted golden nanowires by means of both linear (reflection and absorption) and nonlinear (second harmonic generation) measurements [20-23].

III-V semiconductor nanowires (NWs) have been widely investigated since they exhibit good waveguiding properties thus offering a light manipulation at nanoscale. Coupling of the incident light to the discrete leaky waveguide modes above the bandgap in NWs leads to increased resonant absorption, thus paving the way for important applications such as energy harvesting, spectral selectivity, lasing, spin angular momentum generation etc. [24-27]. Metallic NWs have also been investigated for plasmonic laser applications [28-30] and possibility of surface plasmon polaritons excitation [31]. One step further is the partial covering of such NWs with gold: this can induce, along with the proper experiment set-up, the symmetry breaking which leads to chiral response.

In this paper, for the first time to our knowledge, we report on a circular dichroism behavior from semiconductor hexagonal nanowires partially covered by gold. The NWs were fabricated by means of molecular beam epitaxy on p-Si (111) using a lithography-free oxide patterning. This technique which enables fabrication of highly uniform NW ensembles with tailorable NW density [32]. They were then exposed to a tilted flux of Au that resulted in non-uniform gold layers above the three sides and the tip of the NWs. The light that impinges on such structures under a proper oblique angle will be differently absorbed for circular polarizations of opposite headedness; this optical activity is usually indirectly measured as a difference in power transmitted/reflected by the chiral nanostructure-set-up. More recently, we have shown that photo-acoustic technique can be applied to directly measure circular dichroism in arrays of tilted gold NWs [23] as well as size-dependent resonant absorption properties of semiconductor NWs [33]. Here we apply the same technique to investigate the "extrinsic" chirality in GaAs-based metal-semiconductor hybrid NWs under two wavelengths, 532 nm and 980 nm, corresponding to optical region of different light absorption by GaAs. Such composite material opens several interesting possibilities compared to metal NWs. The semiconductor NW not only acts as a waveguide and scaffolding for the metal structure, but can also effectively convert photons to electron-hole-pairs and vice versa. This property is

3

exploited in NW solar cells, photodetectors, and LEDs by incorporating a pn-junction within the NW. We believe that hybrid nanostructures combining the chiral optical response provided by the asymmetric metal and optoelectronic functionality of the semiconductor NWs can lead to nanophotonic applications in chiral sensing and light manipulation, as well as circular polarization sources.

2. Sample fabrication

The coaxial GaAs-AlGaAs core-shell nanowires were grown by molecular beam epitaxy on p-Si(111) wafers using lithography-free Si/SiOx patterns for defining the nucleation sites. The GaAs core was first grown by self-catalyzed growth mode. Then the Ga catalyst droplet was consumed in As_2-flux in order to terminate axial growth. The $Al_{0.3}Ga_{0.7}As$ shell and GaAs supershell were then grown around the NW core using growth conditions that promote radial growth. The details of the Si/SiOx pattern fabrication and NW growth are explained in details in [24]. The NWs exhibit remarkably phase-pure zincblende crystal structure with the exception of short wurtzite segments formed at the tip of the NW during droplet crystallization when changing from axial to radial growth, see HR-TEM images and HR-XRD spectra on similar samples in our recent paper [34]. The Au film was deposited on the NWs by electron beam evaporation. The incident angle of the Au-flux was $14°$ with respect to the NW axis. The NWs have hexagonal cross-section defined by (110)-facetted sidewalls. One of the (110) facetted NW sidewalls was selected as the azimuthal direction of the Au flux. The nominal Au thickness on this facet is t_{gold_1}=20 nm, while on the neighboring (110) facets the Au thickness is t_{gold_2}=10 nm due to flux geometry.

In Figure 1(a) the tilted $(30°)$ SEM image of 3D distribution of one of the samples (S2 in Table 1) is shown. The 3D schematic and the x-y cross section are shown in Figure 1(b) and 1(c), respectively. Characteristic geometric parameters are the NW length L, the overall

diameter D, AlGaAs shell thickness t_{AlGaAs}, and GaAs supershell thickness t_{GaAs}. In Figure 1(d) x-z cross section from the Au-covered side is shown. The Au cap is shaped depending on the direction of the flux, and its thickness varies from 20 nm to 40 nm. We test three samples having different lengths and diameters in order to experimentally evaluate the dependence of the CD signal to the geometrical parameters of the nanostructures and the fabrication tolerances (see Table 1 for geometrical data of the three samples - the Au evaporation parameters are equal for all the samples).

3. Photo-acoustic technique and linear characterization

We first experimentally characterize our samples by measuring their absorption by means of the photo-acoustic (PA) technique. This technique is based on the generation of heat when a sample absorbs an incoming light beam. If the light intensity is modulated in time, a cycle of heating up and cooling down will correspond to changes in pressure that further produce an acoustic signal. The acoustic signal is then converted into electrical one by a sensitive microphone. This microphone is connected to the cell though a small tunnel, so that the scattered light cannot significantly contribute to PA signal, as shown in the inset of Figure 2(a). Therefore, PA technique directly measures scattering independent absorption in the samples. It has been widely applied to characterize plasmonic nanoparticles and metasurfaces [35-39].

We recently applied this technique to measure the resonant absorption in the NW samples of same geometric parameters before they had been exposed to Au flux [33]. Similar PA set-up is shown in Figure 2(a): the samples are shined from the air side by a Xenon arc lamp source followed by a monochromator, which provides the spectral range from 300 nm to 1100 nm. We show normal incidence absorption spectra for the samples S1-3 in Figure 2(b). The

absorption maxima around 700-800 nm and 450-500 nm originate from HE_{11} and HE_{12} guided

modes present in GaAs-based dielectric hexagonal NWs; however, due to the non-uniform Au

layer, and the interaction between close NWs, these maxima are significantly broadened. To

simulate the absorption cross section of a single GaAs-AlGaAs-GaAs NW covered with Au

we have used Lumerical Finite Difference Time Domain (FDTD). To take into account the

interaction between the closely spaced NWs, we simulate two NWs whose distance is taken

from the nearest neighbour statistics from top SEM images. The good agreement between

numerical and PA spectra allows the assumption that the calculations will fit the PA

experiments for circular incident light too.

4. Chiral absorption results

4.1. PA circular dichroism set-up

Since Au does not uniformly and symmetrically cover the hexagonal NWs, under oblique

incidence, these structures promise to exhibit chiral effects under proper configurations.

Therefore, we change our PA set-up in order to be able to scan polarization and incidence

angles, Figure 3(a). We use two laser wavelengths: 532 nm to report on the range where all of

the NW materials and Au strongly absorb energy, and 980 nm, where GaAs and AlGaAs are

almost non-absorbing, while Au strongly reflects light (Si substrate is the only material that

absorbs at 980 nm). The laser light is polarized before the quarter wave plate, so that it is $\hat{s}$-

polarized when the fast wave plate's axis is at 0°. Fast axis wave plate scans the angles from -

180° to 180°, where −45° represents left-handed circular polarization (CL) and 45° represents

right-handed circular polarization (CR). PA cell is mounted on a rotational stage, which

enables the incidence angle scan from θ=-56º to 56º, as well as four different NW

configurations (see Figure 3(b)); NW primary sidewall covered with Au can be in xz plane

towards y_+ direction (Up configuration), xz plane towards y_- direction (Down

configuration), yz plane towards x_+ direction (Right configuration), and yz plane towards x_-

direction (Left configuration).

4.2. CD dependence on the incidence angle

As a figure of merit that defines the level of circular dichroism in PA measurements, we use:

$$CD[\%] = \frac{A_{CL} - A_{CR}}{A_{CL} + A_{CR}} \cdot 100 \quad , \qquad (1)$$

where A_{CL} (A_{CR}) stands for the PA signal amplitude for CL (CR) polarization. In Figure 4(a)

we show measured (solid lines) and calculated (dashed lines) CD as a function of the incident

angle for the three samples at 532 nm in Up configuration. We see that in all three samples

CD increases from 0% at normal incidence, since both the set up and the structure are

symmetric; in both Left and Right configurations, as well as for NWs samples without the

asymmetric gold cover, CD is negligible, as the circularly polarized light does not see the

symmetry breaking. CD follows the form of the numerically calculated dependence, and the

experimental maximum CD of 8% is reached for S2 at 27°; this sample has the longest L,

while S1 and S3 have similar shorter L, which leads to a smaller CD. Thus, the results of the

measurements in Figure 4(a) indicate that the dominant parameter in CD signal is attributed to

the length of NWs, while the diameter does not have a strong influence on the chiral response.

On the contrary, the diameter strongly affects the linear response of gold-free NWs [33].

However, PA signal has also a high contribution of a non-chiral Si substrate, while the

simulations take into account just its small depth (limited by the calculation region), thus

slightly overestimating CD. We attribute the other discrepancies to the fact that single NW

simulations cannot completely catch the collective behaviour due to the NW interactions and

to the variations of fabrication parameters such as Au cap thickness. In Figure 4(b) the polar

plot of the PA signal is shown for S3 at 532nm in Up configuration (0° corresponds to $\hat{s}$-

polarized light) for different input angles of the impinging light. The difference between the

lobes corresponding to CL and CR is strong at 11º, 18º and 26º, while from 34º this difference decreases. Similar plots have been obtained for S1 and S2 samples.

Since sample S2 gives rise to the higher CD signal, in what follows we perform more detailed measurements on S2 by looking at different experimental geometries.

4.3. CD for Up and Down configurations

In Figure 5(a) we present polar plots of PA signals for the angle of incidence θ=-45º, at 532 nm, for Down (red curve) and Up (blue curve) configurations. As expected from the theory of "extrinsic" chirality, the circular dichroism reverses its sign passing from Up to Down configuration. This influences also on the shape of the electromagnetic field reflected from the structure. In Figure 5(b) we show the calculated reflection far field intensity at θ=45º incidence for CL and CR illumination in Up and Down configurations. Both direction and intensity of the reflected light change in these four combinations with respect the specular reflection direction, which indicates as possible applications of such NWs, the control the direction and intensity of the light.

4.4. Maximum CD at opposite incidence angles

In Figure 6(a) we show PA polar plot for the Down configuration, in the conditions where the maximum CD is achieved which is obtained for the sample S2 at around θ=27º at 532nm (see Figure 4(a)). As expected, the chiral feature shows 90º shift in polarization for the incidence angle of θ=-27º. The "extrinsic" chirality is strong and we see no additional lobes.

It is interesting also to evaluate the field profile in the NW when the CD occurs. In Figure 6(b) the simulations of the electric field intensity are shown if S2 is excited under θ=27º at 532 nm wavelength. For CR the field is concentrated on the gold-covered sidewalls, while for CL it is concentrated on the opposite side. This suggests that these NWs could provide light path and polarization control. In particular, they could enable a completely new approach for

chiral sensing in the form of hot electron Schottky photodetector [40] exploiting the circular polarization dependent plasmonic absorption at GaAs-Au interface.

4.5. Maximum CD at different wavelengths

We further examine the behaviour at two different wavelengths: 532 nm and 980nm. Since at 532 nm both Au and NW materials contribute to the absorption, while at 980 nm NWs are transparent and Au strongly reflects light, we expect CD to be significantly greater at 532 nm. Indeed, angular dependence, gave CD values 50% lower at 980 nm with respect to 532nm. In figure 7 we report the comparison among the polar plots obtained at the above mentioned wavelengths. In figure 7(a) are shown the polar plots of the PA signal obtained on sample S2 in Down configuration for different incidence angles at the wavelength of 532 nm. In figure 7(b) we show the polar plots of the PA signal obtained in the same conditions at the wavelength of 980nm. In Figure 7(c) both numerical (red curve) and experimental (blue curve) PA signal are shown for sample S2 at $\theta=18°$ of incidence at 532nm in Up configuration; in figure 7(d) PA signal in the same condition at the wavelength of 980nm is reported. We see that FDTD numerical simulations can efficiently predict the chiral behaviour of these NW ensembles. This means that we can improve our fabrication parameters to optimize CD at wanted wavelengths, leading to unprecedented applications in chiral NW-based devices.

5. Conclusions

We experimentally investigate the effective chiral behaviour of GaAs-based nanowire ensembles partially covered by gold. The employed fabrication process allows for the fabrication of highly uniform GaAs-AlGaAs NW ensembles; exposing them to the tilted Au flux leads to the asymmetric structure that exhibits CD behaviour. The "extrinsic" chiral

behaviour was confirmed by measuring the differences in absorption for the circular incident light of the opposite headedness. Our scattering-independent PA set-up directly measures the absorption and allows scanning of the incidence angles and polarization. We have measured configurations with different symmetry and incidence angles, under two particular wavelengths, and numerically confirmed results by means of FDTD simulations. NW fabrication parameters can be further easily optimized to improve CD. By testing three samples having different lengths and diameters, we infer that the diameter does not have a strong influence on the chiral response, while the chiral response can be increased with longest sample.

We strongly believe that bringing together the advantages of semiconductor optoelectronics platform, waveguiding properties of vertical NWs and chiral behaviour when their symmetry is broken could lead to the new perspectives in control of the light at nanoscale and in developing new chiral sensing devices. To this end, our current efforts are dedicated to the development of prototype chiral photodectors based on asymmetrically metal coated GaAs NWs including pn-junctions for collecting the charge carriers.

Received: ((will be filled in by the editorial staff))
Revised: ((will be filled in by the editorial staff))
Published online: ((will be filled in by the editorial staff))

References

[1]   J. B. Pendry, *Science* **2004**, *306*, 1353.

[2]   J. Zhou, J. Dong, B. Wang, T. Koschny, M. Kafesaki, and C. M. Soukoulis, *Phys. Rev. B* **2009**, *79*, 121104 (R).

[3]   S. Zhang, Y.Park, J. Li, X. Lu, W. Zhang, and X. Zhang, *Phys. Rev. Lett.* **2009**, *102*, 023901.

[4]   A. Kuzyk, R. Schreiber, Z. Fan, G. Pardatscher, E. Roller, A. Högele, F. C. Simmel, A. O. Govorov, and T. Liedl, *Nature* **2012**, *483,* 311-314.

[5]   Y. He, K. Lawrence, W. Ingram, and Y. Zhao, *Chem. Commun.* **2016**, *52*, 2047-2050.

[6]   A. M. Yao, and M. J. Padgett, *Adv. Opt. Photon.* **2007**, *446*, 3.

[7]   H. K. Bisoyi, and Q. Li, *Acc. Chem. Res.* **2014**, *47* (10), 3184–3195.

[8]   C. Wu,w, N. Arju, G. Kelp, J. A. Fan, J. Dominguez, E. Gonzales, E. Tutuc, I. Brener, and G. Shvets, *Nat. Commun.* **2014**, *5*, 3892.

[9]   V. K. Valev, J. J. Baumberg , B. De Clercq, N. Braz, X. Zheng, E. J. Osley, S. Vandendriessche M. Hojeij, C. Blejean, J. Mertens, C. G. Biris, V. Volskiy, M. Ameloot, Y. Ekinci, G. A. E. Vandenbosch, P. A. Warburton, V. V. Moshchalkov, N. C. Panoiu, and T. Verbiest, *Adv. Mater.* **2014**, *26* (24), 4074-4081.

[10]   V. K. Valev, J. J. Baumberg, C. Sibilia, and T. Verbiest, *Adv. Mater.* **2013**, *25* (18), 2517-2534.

[11]   J. K. Gansel, M. Thiel, M. S. Rill, M. Decker, K. Bade, V. Saile, G. von Freymann, S. Linden, and M. Wegener, *Science* **2009**, *325*, 1513–1515.

[12]   Y. Zhou, M. Yang, K. Sun, Z. Tang, and N. A. Kotov, *J. Am. Chem. Soc.* **2010**, *132* (17), 6006-6013.

[13]   Y. Xia, Y. Zhou, and Z. Tang, *Nanoscale* **2011**, 3, 1375-1382.

[14]   Y. Zhou, Z. Zhu, W. Huang, W. Liu, S. Wu, X. Liu, Y. Gao, W. Zhang, and Z. Tang, *Angew. Chem. Int. Ed.* **2011**, *50*, 11456–11459.

[15]   Y. Li, Y. Zhou, HY Wang, S Perrett, Y Zhao, Z Tang, and G Nie, *Angew. Chem. Int. Ed.* **2011**, *50*, 5860–5864.

[16] Z. Zhu, J. Guo, W. Liu, Z. Li, B. Han, W. Zhang, and Z. Tang, *Angew. Chem. Int. Ed.* **2013**, *52*, 13571–13575.

[17] T. Verbiest, M. Kauranen, Y. Van Rompaey, and A. Persoons, *Phys. Rev. Lett.* **1996**, *77*, 1456-1459.

[18] E. Plum, X.-X. Liu, V. A. Fedotov, Y. Chen, D. P. Tsai, and N. I. Zheludev, *Phys. Rev. Lett.* **2009,** *102*, 113902.

[19] S.N. Volkov, K. Dolgaleva, R.W. Boyd, K. Jefimovs, J. Turunen, Y. Svirko, B. K. Canfield, and M. Kauranen, *Phys. Rev. A* **2009**, *79*, 043819.

[20] M. Bertolotti, A. Belardini, A. Benedetti, and C. Sibilia, J. Opt. Soc. Am. B 2015, 32 (7), 1287-1293.

[21] A. Belardini, M. C. Larciprete, M. Centini, E. Fazio, and C. Sibilia, *Phys. Rev. Lett.* **2011**, *107*, 257401.

[22] A. Belardini, M. Centini, G. Leahu, E. Fazio, C. Sibilia, J. W. Haus, and A. Sarangan, *Faraday Discuss.* **2015**, *178*, 357.

[23] A. Belardini, M. Centini, G. Leahu, D. C. Hooper, R. Li Voti, E. Fazio, J. W. Haus, A. Sarangan, V. K. Valev, and Concita Sibilia, *Sci. Rep.* **2016**, *6*, 31796.

[24] B. Mayer, D. Rudolph, J. Schnell, S. Morkötter, J. Winnerl, J. Treu, K. Müller, G. Bracher, G. Abstreiter, G. Koblmüller, and J. J. Finley, *Nat. Commun.* **2013**, *4*, 2931.

[25] B. Mayer, L. Janker, B. Loitsch, J. Treu, T. Kostenbader, S. Lichtmannecker, T. Reichert, S. Morkötter, M. Kaniber, G. Abstreiter, C. Gies, G. Koblmüller, and J. J. Finley, *Nano Lett.* **2016**, *16* (1), 152–156.

[26] S. Mokkapati, D. Saxena, H. H. Tan, and C. J. Jagadish, *Sci. Rep.* **2015**, *5*, 15539.

[27] M. H. Alizadeh, and B. M. Reinhard, *Opt. Express* **2016**, *24* (8), 8471-8479.

[28] T. P. H. Sidiropoulos, R. Röder, S. Geburt, O. Hess, S. A. Maier, C. Ronning, and R. F. Oulton, *Nature Phys.* **2014**, *10*, 870-876.

[29] X. Wu, Y. Xiao, C. Meng, X. Zhang, S. Yu, Y. Wang, C. Yang, X. Guo, C. Z. Ning, and L. Tong, *Nano Lett.* **2013**, *13*, 5654-5659.

[30] R. F. Oulton, V. J. Sorger, T. Zentgraf, R. Ma, C. Gladden, L. Dai, G. Bartal, and X. Zhang, *Nature Lett.* **2009**, *461*, 629-632.

[31] S. Zhang, H. Wei, K. Bao, Ulf Håkanson, N. J. Halas, P. Nordlander, and H. Xu, *Phys. Rev. Lett.* **2011**, *107*, 096801.

[32] T. V. Hakkarainen, A. Schramm, J. Mäkelä, P. Laukkanen, and M. Guina, *Nanotechnology* **2015**, *26*, 275301.

[33] G. Leahu, E. Petronijevic, A. Belardini, M. Centini, R. Li Voti, T. Hakkarainen, E. Koivusalo, M. Guina, and C. Sibilia, submitted to *Sci. Rep.* **2016**.

[34] E. Koivusalo, T. Hakkarainen, M. Guina, "Structural investigation of uniform ensembles of self-catalyzed GaAs nanowires fabricated by a lithography-free technique",(2017) arXiv:1701.04264 [cond-mat.mes-hall]

[35] R. Inagaki, K. Kagami, and E.T. Arakawa, *Phys. Rev. B* **1981**, *24*, 3644R.

[36] R. Inagaki, K. Kagami, and E.T. Arakawa, *Appl. Opt.* **1982**, 21, 949.

[37] T. El-Brolossy, T. Abdallah, M. Mohamed, S. Abdallah, K. Easawi, S. Negm, and H. Talaat, *Eur. Phys. J. Spec. Top.* **2008**, *153*, 361.

[38] R. Li Voti, G. Leahu, M. C. Larciprete, C. Sibilia, M. Bertolotti, I. Nefedov, and I. V. Anoshkin, *Int. J. Thermophys.* **2015**, *36*, 1342-1348.

[39] S. J. Zelewski, J. Kopaczek, W. M. Linhart, F. Ishikawa, S. Shimomura, and R. Kudrawiec, *Appl. Phys. Lett.* **2016**, *109*, 182106.

[40] Li, Wei, and Jason G. Valentine. "Harvesting the loss: surface plasmon-based hot electron photodetection." *Nanophotonics* 6.1 (2017): 177-191.
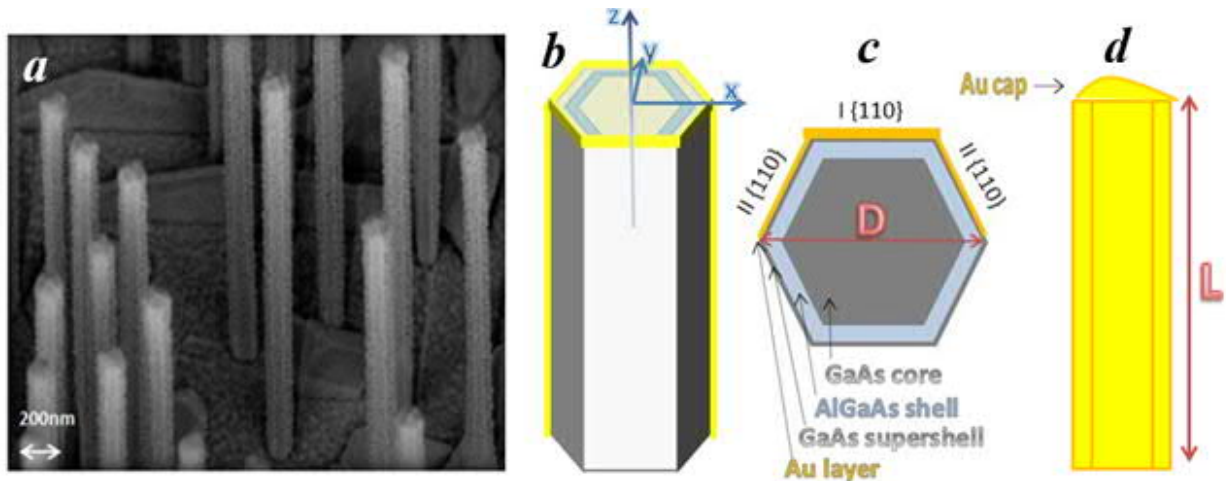
Figure 1. GaAs-based NWs partially covered with Au. (a) Tilted (30°) SEM image of 3D distribution of S2. (b) 3D Schematic of the NW from the side not covered with Au (Au tip is made transparent to show GaAs-AlGaAs-GaAs configuration). (c) x-y cross section with characteristic parameters: overall diameter D, which comprises GaAs core, AlGaAs shell, GaAs supershell. Au layer thickness on the sidewalls depends on the Au flux - the (110) sidewalls in the azimuthal flux direction (I{110}) are t_{gold_1}=20 nm thick, while two other neighboring (110) facets (II{110}) are t_{gold_2}=10 nm thick. (d) x-z cross section from the Au-covered side. The Au cap is shaped depending on the direction of the flux, and its thickness varies from 20 nm to 40 nm.
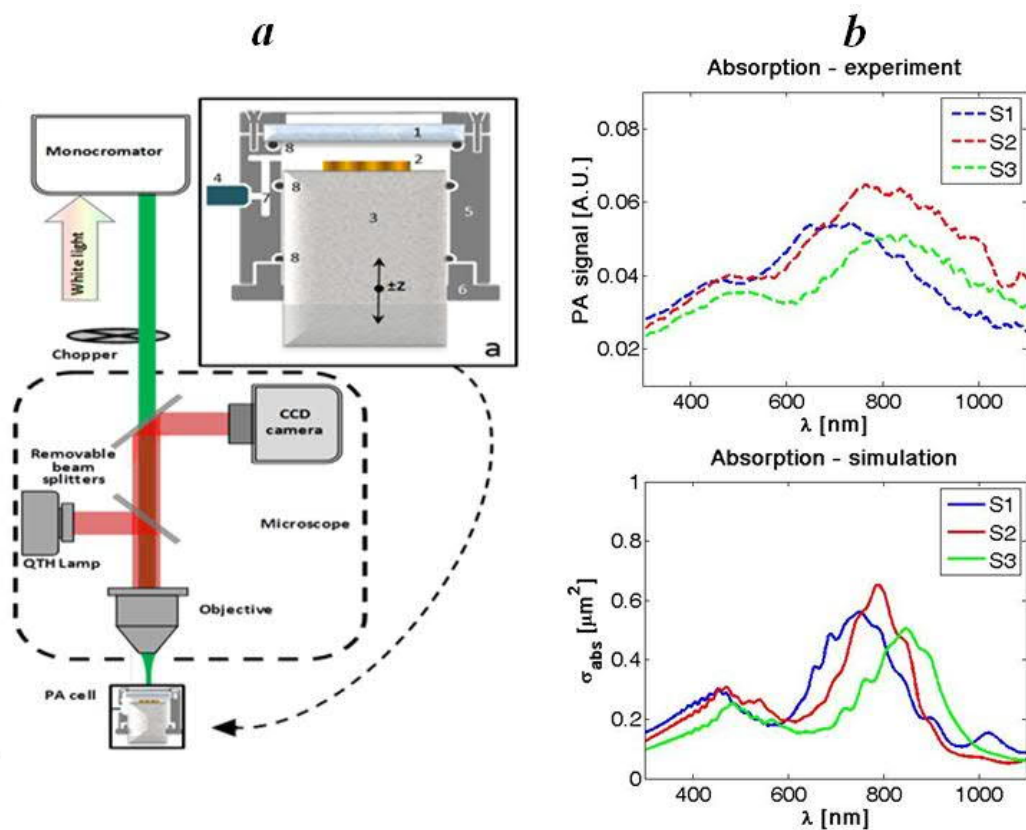
Figure 2. (a) Experimental set-up of the photo-acoustic measurement. Inset (a): Variable volume photoacoustic cell, 1-quartz window, 2-sample, 3-quartz cylinder, 4-microphone, 5-inox cell body, 6-threaded flange, 7-sound labyrinth, 8-O-ring. (b) PA spectra (dashed lines) and simulated absorption cross section (solid lines) of the three samples (S1 blue curves, S2 red curves, S3 green curves).
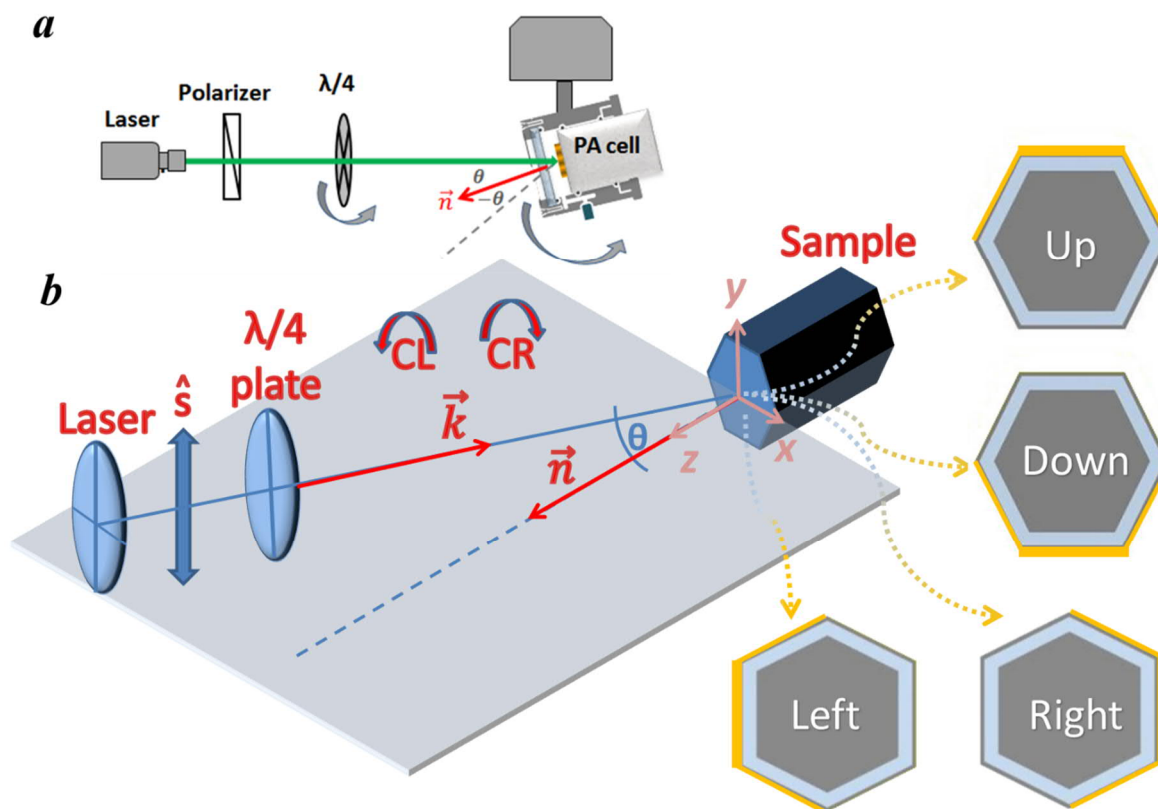
Figure 3. (a) Top view of the circular dichroism measurements set-up. Laser light at the wavelength of 532nm or 980nm is polarized so that it impinges with $\hat{s}$ polarization on a quarter wave plate. Rotational stage allows for the incident angle scan. (b) 3D view of the experiment with four x-y plane configurations when primary I{110} sidewall is in: y_+ region – Up, y_- – Down, x_+ – Right, and x_- – Left.
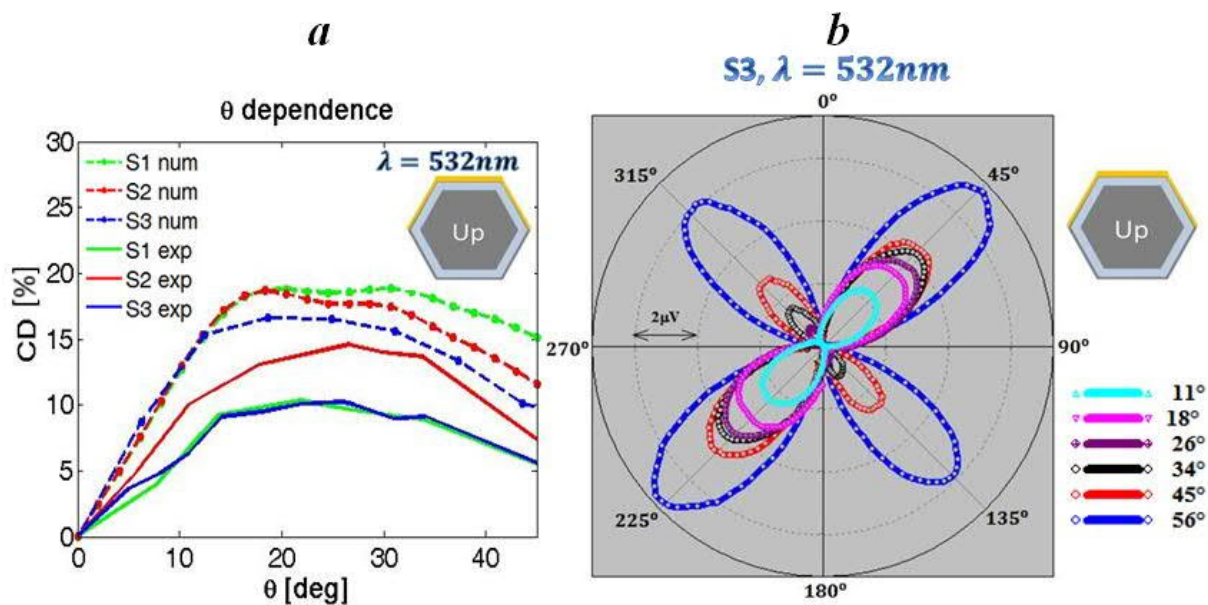
Figure 4. (a) CD incidence angle dependence (experimental measured values in solid lines, numerical values in dashed lines) for the samples S1-3 for the Up configuration at 532nm; Sample S1 in green, S2 in red, S3 in blue. (b) PA polar plots for S3 at 532nm in Up configuration for various angles of incidence : 11° cyan, 18° magenta, 26° violet, 34° black, 45° red, 56° blue.
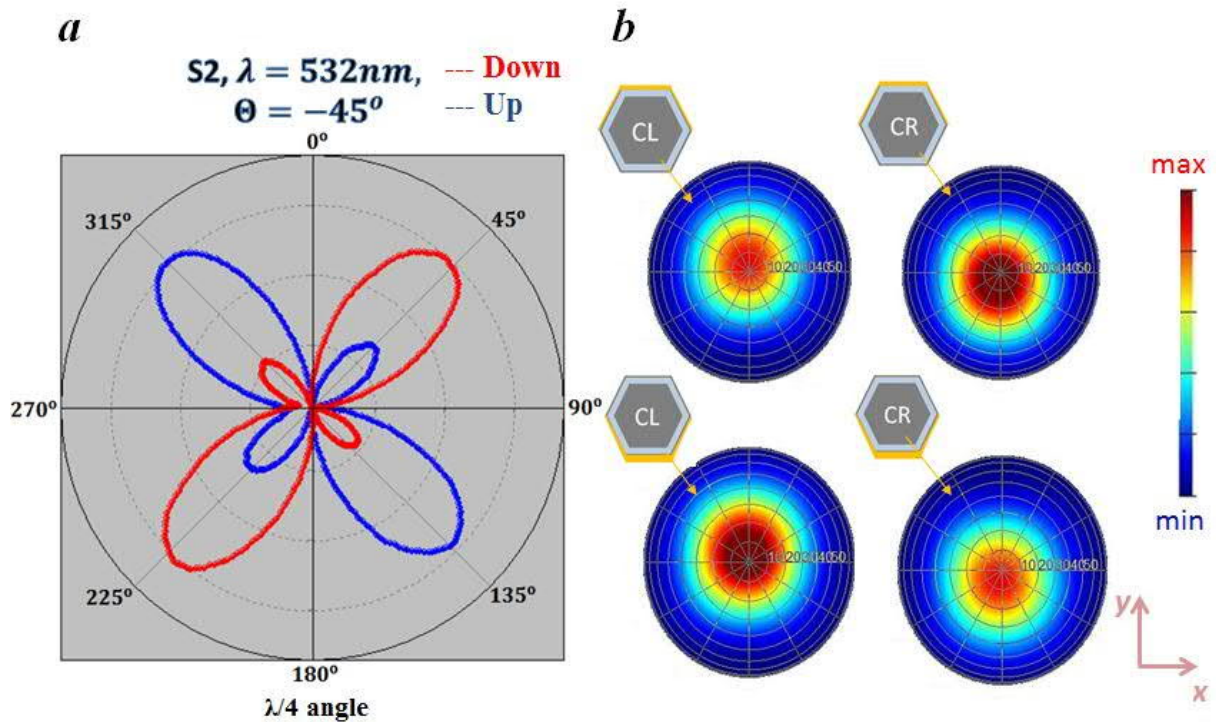
Figure 5. (a) Polar plots of PA signal for Up (blue curve) and Down (red curve) configurations of S2 at 532 nm and -45deg incidence. CD switches sign between the two configurations. (b) Reflection far field intensity at 45º incidence for CL and CR impinging light in Up and Down configurations; we see that changing the input polarization from CL to CR we can control the reflected field intensity and direction (the centers of the plots indicates the specular reflection).
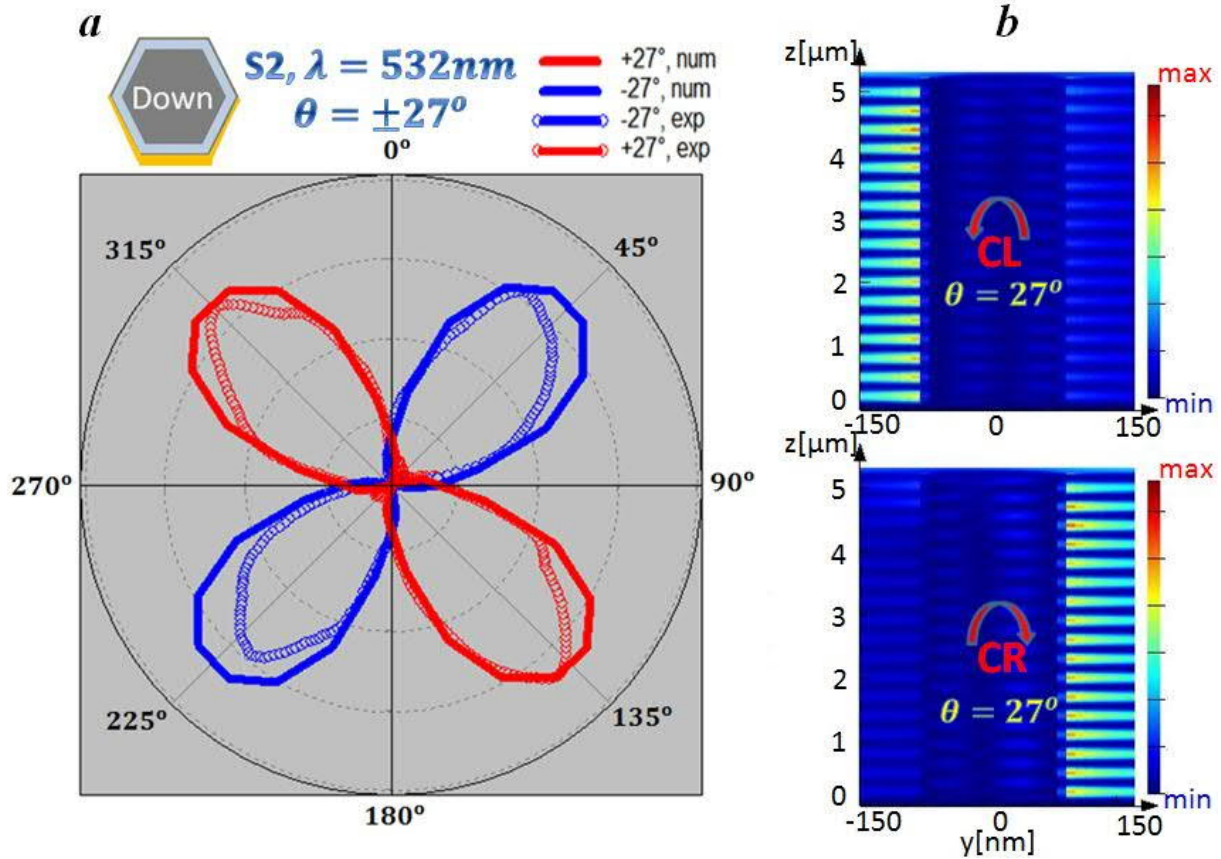
Figure 6. (a) Polar plots (experimental values in open circles and numerical ones in solid lines) for Down configurations of S2 at 532 nm for -27º (blue) and 27º (red) incidence. CD has a 90º shift between these two configurations. (b) Intensity of the electric field in y-z cross section when S2 is excited with CR or CL at 27º.
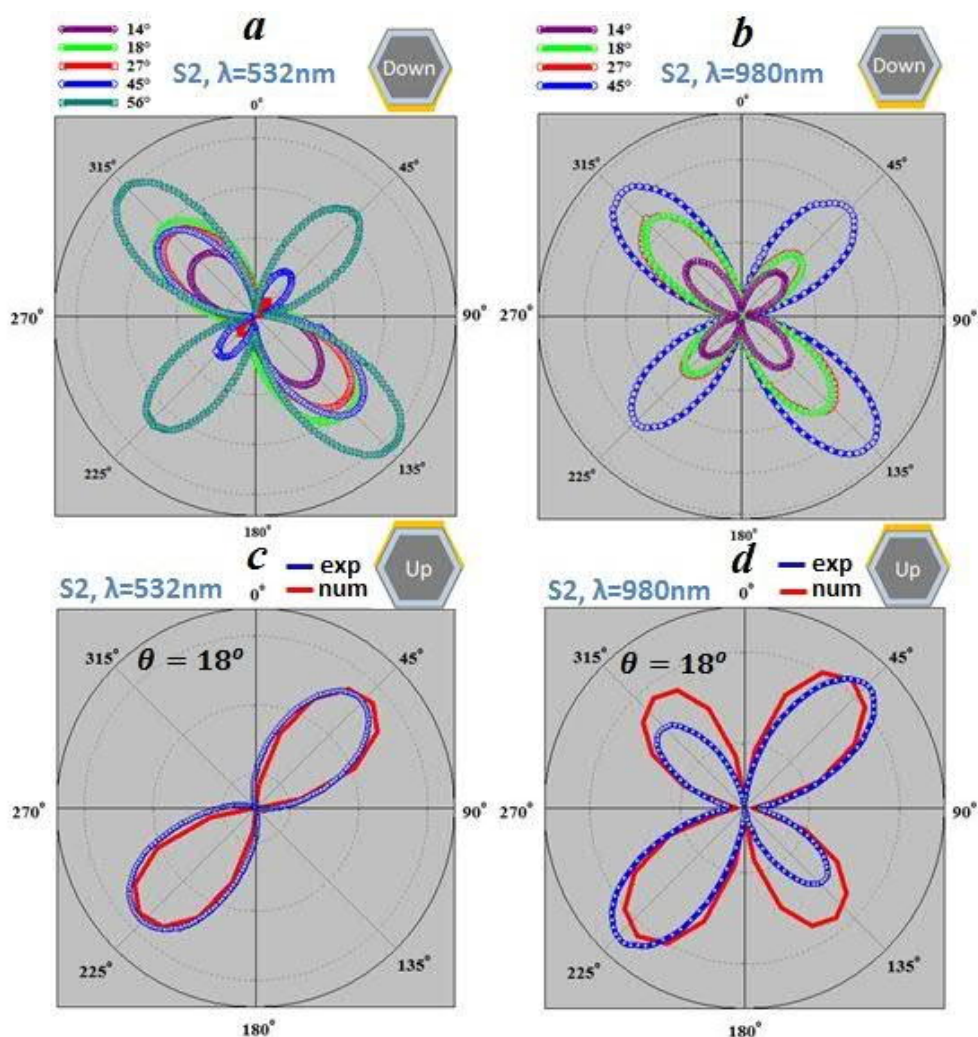
Figure 7. (a) polar plots of the PA signal obtained on sample S2 in Down configuration for different incidence angles at the wavelength of 532nm. (b) polar plots of the PA signal obtained on sample S2 in Down configuration for different incidence angles at the wavelength of 980nm. (c) numerical (red curve) and experimental (blue curve) PA signal for sample S2 at 18° of incidence at 532nm in Up configuration. (d) numerical (red curve) and experimental (blue curve) PA signal are shown for sample S2 at 18° of incidence at 980nm in Up configuration.

Table 1. Characteristic geometric parameters for the three samples together with their standard deviations. The samples exhibit low fabrication error margins.

Sample	L [nm]	D [nm]	t_{AlGaAs} [nm]	t_{GaAs} [nm]	t_{gold_1} [nm]	t_{gold_2} [nm]
S1	4750±34	138±5	3.5	0.7	20	10
S2	5190±64	151±5	8.6	1.7	20	10
S3	4600±52	165±6	11.7	5.8	20	10

WILEY-VCH